NASA CONTRACTOR REPORT

NASA CR-2396

NASA CR-2396

RADIATION AND SCATTERING BY THIN-WIRE STRUCTURES IN THE COMPLEX FREQUENCY DOMAIN

by J. H. Richmond

Prepared by
THE OHIO STATE UNIVERSITY
ELECTROSCIENCE LABORATORY
Columbus, Ohio 43212
for Langley Research Center

NATIONAL AERONAUTICS AND SPACE ADMINISTRATION • WASHINGTON, D. C. • MAY 1974

1. Report No.	2. Government Accession No.	3. Recipient's Catalog No.
NASA CR- 2396		

4. Title and Subtitle	5. Report Date
RADIATION AND SCATTERING BY THIN-WIRE STRUCTURES IN THE COMPLEX FREQUENCY DOMAIN	May 1974
	6. Performing Organization Code
7. Author(s)	8. Performing Organization Report No.
J. H. Richmond	TR 2902-10
	10. Work Unit No.
9. Performing Organization Name and Address	502-33-13-01
The Ohio State University	11. Contract or Grant No.
ElectroScience Laboratory	NGL 36-008-138
Columbus, Ohio 43212	13. Type of Report and Period Covered
12. Sponsoring Agency Name and Address	Contractor Report
National Aeronautics and Space Administration	14. Sponsoring Agency Code
Washington, D.C. 20546	

15. Supplementary Notes

Topical report

16. Abstract

Piecewise-sinusoidal expansion functions and Galerkin's method are employed to formulate a solution for an arbitrary thin-wire configuration in a homogeneous conducting medium. The analysis is performed in the real or complex frequency domain. In antenna problems, the solution determines the current distribution, impedance, radiation efficiency, gain and far-field patterns. In scattering problems, the solution detemines the absorption cross section, scattering cross section and the polarization scattering matrix. This report presents the electromagnetic theory for thin wires and develops the forward-scattering theorem for an arbitrary target in a homogeneous conducting medium.

17. Key Words (Suggested by Author(s))	18. Distribution Statement
Antennas, Spacecraft and Aircraft Antennas Applied Electromagnetic Theory	Unclassified - Unlimited STAR Category 09

19. Security Classif. (of this report)	20. Security Classif. (of this page)	21. No. of Pages	22. Price*
Unclassified	Unclassified	41	$3.25

*For sale by the National Technical Information Service, Springfield, Virginia 22151

CONTENTS

I. INTRODUCTION

In 1932 Carter[1] used the induced emf formulation and a sinusoidal current distribution to derive expressions for the mutual impedance between half-wave dipoles. H.E. King[2] extended these results in 1957 to parallel dipoles in echelon with arbitrary wire lengths. Baker and LaGrone[3] employed numerical integration for skew dipoles.

These two-segment sinusoidal solutions have been useful for coupled dipoles with lengths up to about 0.5λ. In this range, the current distribution on each thin-wire antenna is in most cases not greatly disturbed by the other. More sophisticated techniques are required, however, for longer antennas and for more complex wire configurations. One approach is to reduce the integral equation to a system of simultaneous linear equations. The unknown constants in these equations are usually samples of the current function $I(\ell)$ or the coefficients in a modal expansion for the current distribution.

In 1967 Yeh and Mei[4] employed such techniques to analyze the conical-spiral antenna. Programs for arbitrary thin-wire configurations were developed by Tanner and Andreasen[5], Miller and Morton[6], Chao and Strait[7], and Richmond[8,9,10,11,12]. In References 4, 5 and 6 the current distribution on each wire segment has the form $I = A + B \cos k\ell + C \sin k\ell$. Reference 7 uses a piecewise-linear expansion. References 8 through 12 use a piecewise-sinusoidal expansion with $I = A \cos k\ell + B \sin k\ell$. Others who have employed the piecewise-sinusoidal expansion include Butler[13] and Imbriale and Ingerson[14].

This paper presents the electromagnetic theory for thin-wire antennas and scatterers. The ambient medium is considered to be isotropic, linear and homogeneous. The analysis is performed in the frequency domain, and the generator or incident wave may have a real or complex frequency. The solution satisfies Kirchhoff's current law on the wire structure, and has favorable properties of convergence and computational efficiency. The computer programs will be presented in a future report.

With no significant loss of generality, the wire structure is considered to be a generalized polygon assembled from straight wire segments. The formulation and the program have been tested extensively in radiation and scattering problems with various dipoles, loops, arrays and wire-grid models of plates, spheres, cones, aircraft and ships. Although the air-earth or air-water interface is not considered, the theory and program are useful in many situations involving buried or submerged antennas and scatterers.

A piecewise-sinusoidal expansion is used for the current distribution. The matrix equation Z I = V is generated by enforcing reaction tests with a set of sinusoidal dipoles located in the interior region of the wire. Since the test dipoles have the same current distribution as the expansion modes, this may be regarded as an application of Galerkin's method[15]. However, the physical ideas of Rumsey's reaction concept[16] were more inspirational in this development than the mathematical ideas of the moment method.

On each thin-wire structure, we define a set of terminals or current-sampling points. Terminals are defined at each corner or bending point, at each junction where several straight wires intersect, and at the wire endpoints. For accuracy, no segment should have a length much greater than $\lambda/4$. Thus, a long segment may be subdivided by defining additional sampling points.

With several terminals defined in this manner, the wire structure is a multiport system. The elements in the open-circuit impedance matrix are calculated by numerical integration when appropriate, or by closed-form expressions in terms of exponential integrals. The impedance matrix is inverted to obtain the short-circuit admittance matrix.

The sinusoidal reaction formulation was developed earlier for wire structures in free space. The generalization to wires in a conducting medium with complex frequency is based on electromagnetic similitude and analytic continuation.

The next section presents the reaction integral equation for thin wires. The remaining text defines the sinusoidal expansion and testing functions and develops the theory for wire structures with lumped loading and finite conductivity. The forward-scattering theorem is considered for a target in a conducting medium, and numerical results are displayed for the echo area, radiation efficiency and impedance of a straight wire in a conducting medium. As an example of a nonplanar structure with four straight wires intersecting at a junction, we present some poles of the admittance function of a "regular quadripod", plotted on the complex gamma plane. Appendices consider the near-zone and far-zone fields of sinusoidal line sources.

II. THE REACTION INTEGRAL EQUATION

Let S denote the closed surface of the wire structure, and let V denote the interior volumetric region. In the presence of the wire, an external source $(\underline{J}_i, \underline{M}_i)$ generates the field $(\underline{E}, \underline{H})$. When radiating in the homogeneous medium (μ, ε) without the wire, this source generates the incident field $(\underline{E}_i, \underline{H}_i)$. The scattered field is defined as follows:

(1) $$\underline{E}_s = \underline{E} - \underline{E}_i$$

(2) $$\underline{H}_s = \underline{H} - \underline{H}_i$$

These fields are considered to be time-harmonic with the same frequency. The time dependence $e^{j\omega t}$ or e^{st} is suppressed.

From the surface-equivalence theorem of Schelkunoff[17], the interior field will vanish without disturbing the exterior field $(\underline{E},\underline{H})$ if we introduce the following surface-current densities

(3) $$\underline{J}_s = \hat{n} \times \underline{H}$$

(4) $$\underline{M}_s = \underline{E} \times \hat{n}$$

on the surface S. (The unit vector $\hat{n}$ is directed outward on S.) In this situation, we may replace the wire structure with homogeneous medium (μ,ε) without disturbing the field anywhere. When $\underline{J}_s$ and $\underline{M}_s$ radiate in the homogeneous medium, they generate the field $(\underline{E}_s,\underline{H}_s)$ in the exterior and $(-\underline{E}_i,-\underline{H}_i)$ in the interior region.

Now let us place a test source (or probe) in the interior region V and consider its reaction with the other sources. If the test source has electric current density $\underline{J}_m$ and magnetic current dentsity $\underline{M}_m$,

(5) $$\iint (\underline{J}_m \cdot \underline{E}_s - \underline{M}_m \cdot \underline{H}_s) ds = - \iint (\underline{J}_m \cdot \underline{E}_i - \underline{M}_m \cdot \underline{H}_i) ds$$

In Eq. (5) $(\underline{E}_s,\underline{H}_s)$ denotes the field generated by $(\underline{J}_s,\underline{M}_s)$, and the integrals extend over the surface of the test source. Equation (5) is one form of the reaction integral equation (RIE). If we enforce Eq. (5) with a set of delta-function electric test sources, the RIE reduces to the well-known electric field integral equation (EFIE). If we enforce Eq. (5) with a set of delta-function magnetic test sources, the RIE reduces to the well-known magnetic field integral equation (MFIE). Thus, the RIE is more general than the EFIE or the MFIE. In other words, Eq. (5) states that the interior test source has zero reaction with the other sources.

From Eq. (5) and the reciprocity theorem, we obtain another form of the reaction integral equation:

$$(6)\qquad \oiint_S (\underline{J}_s \cdot \underline{E}^m - \underline{M}_s \cdot \underline{H}^m)ds + \iiint (\underline{J}_i \cdot \underline{E}^m - \underline{M}_i \cdot \underline{H}^m)dv = 0$$

where $(\underline{E}^m, \underline{H}^m)$ is the field of the test source radiating in the homogeneous medium. This reaction integral equation was developed by Rumsey[16] in 1954. For thin-wire problems, we shall employ Eq. (6) with electric test sources.

In the wire structure, let each segment have a circular cylindrical surface. At each point on the composite cylindrical surface of the wire, it is convenient to define a right-handed orthogonal coordinate system with unit vectors $(\hat{n},\hat{\phi},\hat{\ell})$ where $\hat{n}$ is the outward normal vector, $\hat{\ell}$ is directed along the wire axis and

$$(7)\qquad \hat{\phi} = \hat{\ell} \times \hat{n} \quad .$$

Thus $(\hat{n},\hat{\phi},\hat{\ell})$ correspond directly with the unit vectors $(\hat{\rho},\hat{\phi},\hat{z})$ usually employed in the circular-cylindrical coordinate system.

To simplify the integral equation, we assume the wire radius "a" is much smaller than the wavelength λ, and the wire length is much greater than the radius. Furthermore, we shall neglect the integrations over the flat end surfaces of the wire, neglect the circumferential component J_ϕ of the surface-current density, and consider the axial component J_ℓ to be independent of ϕ. (For thick wires, a more detailed treatment is essential for the ϕ-dependent current modes and the integrations over the junction regions and the open ends of the wire. A more elaborate formulation may also be required if one wire passes within a few diameters of another, or if a wire is bent to form a small acute angle.) In view of these approximations the current density on the wire structure is related to the current as follows:

$$(8)\qquad \underline{J}_s(\ell) = \frac{\hat{\ell} I(\ell)}{2\pi a} = \frac{\underline{I}(\ell)}{2\pi a}$$

where ℓ is a metric coordinate measuring position along the wire axis, and $I(\ell)$ is the total current (conduction plus displacement).

On a perfectly conducting wire, the magnetic current density $\underline{M}_s$ vanishes. If the wire has finite conductivity, we take

$$(9)\qquad \underline{E} = Z_s \underline{J}_s$$

for the tangential electric field on S, where Z_s is the surface impedance for exterior excitation. From Eqs. (4), (7), (8) and (9),

$$(10) \qquad \underline{M}_s = Z_s \underline{J}_s \times \hat{n} = \frac{\hat{\phi}\, Z_s I(\ell)}{2\pi a}$$

By virtue of Eqs. (8) and (10), Eq. (6) reduces to

$$(11) \qquad -\int_0^L I(\ell)(E^m_\ell - Z_s H^m_\phi)d\ell = V_m$$

where L denotes the overall wire length and

$$(12) \qquad V_m = \iiint (\underline{J}_i \cdot \underline{E}^m - \underline{M}_i \cdot \underline{H}^m)dv$$

$$(13) \qquad E^m_\ell = \frac{1}{2\pi} \int_0^{2\pi} \hat{\ell} \cdot \underline{E}^m \, d\phi$$

$$(14) \qquad H^m_\phi = \frac{1}{2\pi} \int_0^{2\pi} \hat{\phi} \cdot \underline{H}^m \, d\phi$$

The sinusoidal reaction formulation for thin wires is based on the integral Equation (11). In this equation the known quantities are $\underline{E}^m$, $\underline{H}^m$, V_m and Z_s. The current distribution $I(\ell)$ is regarded as an unknown function. To permit a solution for the current distribution, the following sections define suitable test sources and expansion modes.

III. THE SINUSOIDAL TEST SOURCES

For a test source we choose a filamentary electric dipole with a sinusoidal current distribution. This is not a wire dipole, but merely an electric line source in the homogeneous medium. The sinusoidal dipole is probably the only finite line source with simple closed-form expressions for the near-zone fields. (See the Appendices.) Furthermore, the mutual impedance between two sinusoidal dipoles is available in terms of exponential integrals, and the piecewise-sinusoidal function is evidently close to the natural current distribution on a perfectly conducting thin wire. These factors governed the choice of test sources.

A typical test source is a V dipole with unequal arm lengths and terminals at the vertex. The current is zero at the endpoints and rises sinusoidally to a maximum at the terminals. The terminal current is one ampere, and the current distribution has a slope discontinuity at the terminals.

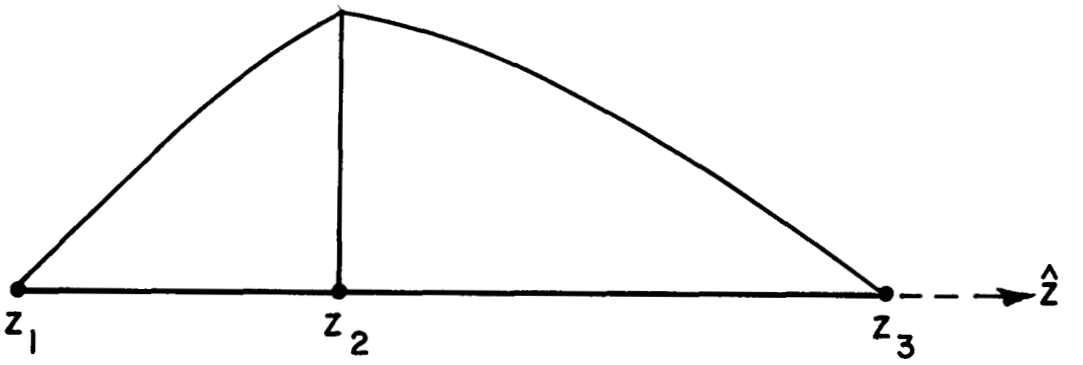

Fig. 1. A linear test dipole and its sinusoidal current distribution. The endpoints are at z_1 and z_3 with terminals at z_2.

For the linear test dipole illustrated in Fig. 1, the current distribution is $\underline{I}(z) = \underline{F}(z)$ where

$$(15) \qquad \underline{F}(z) = \frac{\hat{z}\, P_1 \sinh \gamma(z-z_1)}{\sinh \gamma d_1} + \frac{\hat{z}\, P_2 \sinh \gamma(z_3-z)}{\sinh \gamma d_2}$$

$P_1(z)$ is a pulse function with unit value for $z_1 < z < z_2$ and zero value elsewhere. The pulse function P_2 has unit value for $z_2 < z < z_3$ and vanishes elsewhere. The segment lengths are $d_1 = z_2 - z_1$ and $d_2 = z_3 - z_2$. The current distribution on a V test dipole is

$$(16) \qquad \underline{F}(\ell) = \frac{\hat{\ell}_1\, P_1 \sinh \gamma(\ell-\ell_1)}{\sinh \gamma d_1} + \frac{\hat{\ell}_2\, P_2 \sinh \gamma(\ell_3-\ell)}{\sinh \gamma d_2}$$

In Eqs. (15) and (16), γ denotes the complex propagation constant of the homogeneous exterior medium:

$$(17) \qquad \gamma = s\sqrt{\mu\epsilon}$$

It is only with this value for γ that the sinusoidal test sources have the advantages mentioned earlier.

The test dipole is located in the interior region of the wire structure. To simplify the integrations in Eqs. (13) and (14), we place the test dipole on the wire axis.

A typical problem requires not just one but several test dipoles located at different positions along the wire axis to form an overlapping array. When test dipole m radiates in the homogeneous medium, it generates the field $(\underline{E}^m, \underline{H}^m)$. Each test dipole has the same frequency as the true source. Using N test dipoles, Eq. (11) is enforced for each one. Thus, Eq. (11) represents a system of N simultaneous integral equations with m = 1,2,··N. In other words, Eq. (11) requires each test dipole in the array to have the correct reaction with the true source.

IV. THE SINUSOIDAL EXPANSION FUNCTIONS

The current distribution on the wire structure is expanded in a finite series as follows:

$$\underline{I}(\ell) = \sum_{n=1}^{N} I_n \underline{F}_n(\ell) \tag{18}$$

where the normalized expansion functions $\underline{F}_n(\ell)$ are the same as the test-dipole current distributions in Eq. (16). Since each expansion function extends over just a two-segment portion of the wire structure, these functions are subsectional bases. Since N is finite, Eq. (18) may be considered either as an expansion or an approximation, depending on the context. In Eq. (18), the coefficients I_n are complex constants which represent samples of the current function $I(\ell)$. If the wire segments are short in comparison with the wavelength, the sinusoidal bases resemble the triangular bases of the piecewise-linear model.

Figure 2 illustrates a current distribution $I(\ell)$, its two-mode approximation $I'(\ell)$ and the normalized expansion functions $F_1(\ell)$ and $F_2(\ell)$. It may be noted that $I(\ell)$ is a smooth function except at generators, lumped loads and wire corners. The piecewise-sinusoidal expansion has slope discontinuities at these appropriate locations and also at each intermediate sampling point. With favorable circumstances, the calculated samples I_n will be accurate and the corresponding piecewise-sinusoidal current distribution $I'(\ell)$ will be satisfactory for far-field calculations. For near-zone field analysis, however, one may abandon the sinusoidal interpolation and model the current distribution $I(\ell)$ with a smooth function fitting the calculated samples. In this process, one should <u>not</u> smooth out the slope discontinuities at the generators, lumped loads or wire corners.

By inserting Eq. (18) into Eq. (11), we obtain the following system of simultaneous linear algebraic equations:

(19) $$\sum_{n=1}^{N} I_n Z_{mn} = V_m \qquad \text{where} \quad m = 1,2,\cdots N$$

(20) $$Z_{mn} = - \int_n F_n(\ell) \, (E_\ell^m - Z_s H_\phi^m) \, d\ell$$

In Eq. (20), the integral extends over the two segments in the range of the expansion mode F_n. Equation (19) can be expressed in matrix form as Z I = V where Z denotes the square impedance matrix, I is the current column and V is the voltage column.

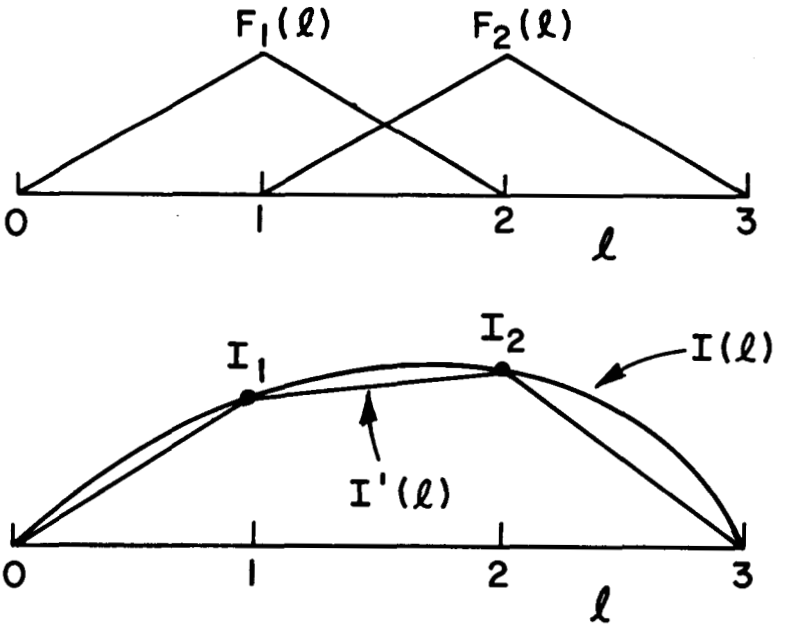

Fig. 2. The expansion functions $F_1(\ell)$ and $F_2(\ell)$, the current distribution $I(\ell)$ and the two-mode approximation $I'(\ell)$.

V. THE IMPEDANCE MATRIX

The elements in the open-circuit impedance matrix are denoted Z_{mn}. By convention, the first and second subscripts indicate the row and column, respectively. Thus, Z_{mn} denotes the mutual impedance between test dipole m and expansion mode n.

The expansion modes form an array of overlapping tubular dipoles located on the wire surface. Each tubular dipole has a sinusoidal distribution of electric surface-current density and an associated magnetic surface-current density. If the test dipoles had the same shapes and positions as the expansion dipoles, the reciprocity theorem could be invoked to demonstrate the symmetry of the impedance matrix. Since the filamentary test dipoles differ from the tubular expansion dipoles, our impedance matrix is not precisely symmetric.

In practice, we regain symmetry by taking a short-cut in calculating the elements in the impedance matrix. From Eqs. (13), (14) and (20), Z_{mn} is expressed as an integration over the composite circular-cylindrical surface of the tubular expansion dipole n. The short-cut is accomplished by approximating the surface integral with a line integral. Thus, to reduce computational costs, we approximate Z_{mn} by the mutual impedance between two filamentary V dipoles, one located on the wire axis and the other on the wire surface. For a straight wire, the mutual impedance is independent of the circumferential position of the dipole located on the surface. For a bent wire, however, the mutual impedance is sometimes quite sensitive to the circumferential position. Via numerical experiments, we have found a suitable position such that the circumferential integrations in Eqs. (13) and (14) are adequately approximated from a single sample of the integrand.

With the approximation mentioned above, the impedances Z_{mn} are given by classical induced emf theory[1,2,3]. The line integral in Eq. (20) is usually performed with numerical integration. When dipoles m and n are close together, however, a closed-form expression (in terms of exponential integrals) is employed for Z_{mn}.

VI. LUMPED LOADS

Suppose a lumped impedance Z_m is inserted in the wire structure at each of the current sampling points. These linear impedances may be active or passive, identical or assorted. The current through the load Z_m is denoted by I_m, and the voltage drop across the load is $I_m Z_m$. The effect is the same as that of a voltage generator with voltage $I_m Z_m$. Thus, a detailed analysis of a lumped load will involve a magnetic frill, ring or tube as in Section 8.

In the simplest model, the delta gap, the lumped loads simply introduce a new term in Eq. (19) so the right-hand side becomes $V_m - I_m Z_m$. Transposing the last term, we obtain

$$(21) \qquad \sum_{n=1}^{N} I_n \overline{Z}_{mn} = V_m$$

With the delta-gap model, the matrix $\overline{Z}_{mn}$ is the same as Z_{mn} with the exception of the diagonal elements which are

$$\overline{Z}_{mm} = Z_{mm} + Z_m \tag{22}$$

Thus, the effect of lumped loading is accounted for simply by modifying the elements in the square impedance matrix. If the above delta-gap approximation is employed, the matrix $\overline{Z}_{mn}$ will have the same symmetry properties as Z_{mn}.

VII. WIRES WITH FINITE CONDUCTIVITY

The surface impedance Z_s will vanish unless the wire has finite conductivity. From Eq. (20),

$$Z_{mn} = Z'_{mn} - \int_n F_n \, E^m_\ell \, d\ell \tag{23}$$

where

$$Z'_{mn} = Z_s \int_n F_n \, H^m_\phi \, d\ell \tag{24}$$

Although longitudinal inhomogeneities in the surface impedance and wire radius offer no difficulties, it is assumed in Eq. (24) and hereafter that these parameters are independent of ℓ. The integral in Eq. (24) extends over the two wire segments in the range of expansion mode F_n. From Eq. (14) and Ampere's law, a suitable approximation is

$$H^m_\phi = \frac{F_m(\ell)}{2\pi a} \tag{25}$$

$$Z'_{mn} = \frac{Z_s}{2\pi a} \int_{m,n} F_n(\ell) \, F_m(\ell) d\ell \tag{26}$$

where region (m,n) is the wire surface shared by dipoles m and n. This region covers two intersecting segments if m and n are equal. If m and n differ, the shared region covers at most one wire segment. For a diagonal element, m and n are equal and Eqs. (16) and (26) yield

$$(27) \qquad Z'_{mm} = \frac{Z_s}{8\pi\gamma a}\left[\frac{\sinh(2\gamma d_1)-2\gamma d_1}{\sinh^2 \gamma d_1} + \frac{\sinh(2\gamma d_2)-2\gamma d_2}{\sinh^2 \gamma d_2}\right]$$

where d_1 and d_2 are the lengths of the two wire segments occupied by mode m. For an off-diagonal element, a suitable approximation is $Z'_{mn} = 0$ if modes m and n do not share a segment. If they share one segment and have terminals at the same end of this segment (length d),

$$(28) \qquad Z'_{mn} = \frac{[\sinh(2\gamma d)-2\gamma d]Z_s}{8\pi\gamma a \sinh^2 \gamma d}$$

If modes m and n share one segment and have terminals at opposite ends of this segment,

$$(29) \qquad Z'_{mn} = \frac{(\gamma d \cosh \gamma d - \sinh \gamma d)Z_s}{4\pi\gamma a \sinh^2 \gamma d}$$

If $\underline{F}_m$ and $\underline{F}_n$ are antiparallel on the shared segment, a minus sign must be inserted on the right-hand side of Eqs. (28) or (29).

If Eq. (26) is employed, it is obvious that the square matrix Z'_{mn} will be symmetric. From Eq. (23) and the reciprocity theorem, the matrix Z_{mn} (and $\bar{Z}_{mn}$ with lumped loading) will also be symmetric if the tubular expansion dipoles are approximated by filamentary dipoles located on the wire surface. This symmetry alleviates computational expenses and storage requirements.

VIII. INSULATED WIRES

For a wire antenna in a conducting medium, the radiation efficiency can often be improved by insulating all or part of the wire from the medium. This is accomplished with a thin dielectric layer coated on the wire surface. This section considers the electromagnetic modeling of the dielectric layer or shell.

Although the surface-impedance model is simple to program, there is some uncertainty regarding its adequacy in this application. Therefore, let us consider a rigorous alternative model.

For simplicity, let the dielectric shell have the same permeability as the ambient medium. From the volume equivalence theorem (Section 11) the dielectric shell may be replaced with ambient medium and an equivalent source with electric current density

$$\underline{J} = j\omega(\varepsilon_2 - \varepsilon)\,\underline{E} \tag{30}$$

where $\underline{E}$ denotes the electric field intensity in the shell and ε_2 and ε are the complex permittivities of the shell and the ambient medium respectively. From Eq. (30), the current $\underline{J}$ vanishes outside the region of the dielectric shell.

Let $(\underline{E},\underline{H})$ denote the field generated by $(\underline{J}_i,\underline{M}_i)$ in the presence of the insulated wire. Outside the wire, this field may also be generated by $(\underline{J}_i,\underline{M}_i)$, $(\underline{J}_S,\underline{M}_S)$ and $\underline{J}$, radiating in the homogeneous medium. These sources, radiating in the homogeneous medium, generate a null field in the interior region of the wire. The surface currents $(\underline{J}_S,\underline{M}_S)$ are located on the surface of the wire and are related to the field $(\underline{E},\underline{H})$.

For the insulated wire, the reaction integral equation (Eq. (6)) is modified by replacing $\underline{J}_i$ with $\underline{J}_i + \underline{J}$. The current $\underline{J}$ may be regarded as an additional source which plays much the same role as the impressed source $\underline{J}_i$. However, $\underline{J}_i$ is considered to be a known source whereas $\underline{J}$ is unknown because $\underline{E}$ is unknown. If the dielectric shell is thin, $\underline{J}$ may be regarded as a dependent unknown function because it is simply related to the current distribution on the wire.

If the wire has large or perfect conductivity, the electric field at the wire surface will be essentially in the radial direction, and E_ρ can be determined from the charge density on the wire surface. For a thin shell on a highly conducting wire, a suitable approximation for the field in the shell is

$$\underline{E} = \frac{-\hat{\rho}\ I'}{2\pi j\omega\varepsilon_2\rho} \qquad \text{where } I' \text{ denoted } dI/d\ell \tag{31}$$

From Eqs. (30) and (31),

$$\underline{J} = \frac{-(\varepsilon_2 - \varepsilon)\hat{\rho}\ I'}{2\pi\ \varepsilon_2\ \rho} \tag{32}$$

For an insulated wire, each expansion mode $\underline{F}_n(\ell)$ has associated with it a shell of radial electric current $\underline{J}$. Thus, the mutual impedance Z_{mn} between the filamentary test dipole m and the tubular expansion dipole n has an additional term given by

$$(33) \qquad \Delta Z_{mn} = \frac{(\varepsilon_2 - \varepsilon)}{\varepsilon_2} \iint_n F'_n(\ell)\, E^m_\rho \, d\rho \, d\ell$$

where the integration extends through the dielectric shell in the range of the expansion dipole n. In deriving Eq. (33), the integration on ϕ was performed with the assumption that $\underline{J}$ and E^m_ρ are independent of ϕ. In integrating on ρ, the limits are a and b which denote the inner and outer radii of the dielectric shell.

In the dielectric shell, the test-dipole field E^m_ρ may be approximated by

$$(34) \qquad E^m_\rho = \frac{-F'_m}{2\pi\, j\omega\varepsilon\rho}$$

In Eq. (33) or (34), ρ denotes distance from the axis of dipole n or m, respectively. Furthermore, the vector direction of the field component E^m_ρ in Eq. (33) generally differs from that in Eq. (34) unless dipoles m and n are coaxial. If Eq. (34) is employed, Eq. (33) reduces to

$$(35) \qquad \Delta Z_{mn} = -\frac{(\varepsilon_2 - \varepsilon)\, \ell n(b/a)}{2\pi\, j\omega\varepsilon\ \varepsilon_2} \int_{m,n} F'_m(\ell)\, F'_n(\ell)\, d\ell$$

where (m,n) denotes the region of ℓ shared by dipoles m and n. The approximate result represented by Eq. (35) yields a matrix ΔZ_{mn} which is symmetric even when some of the wire segments are insulated and others are bare.

In the sinusoidal reaction formulation, insulation is accounted for entirely through a modification of the square impedance matrix Z_{mn}. This modification influences the current distribution, impedance, efficiency, field patterns and scattering properties. The polarization current $\underline{J}$ generates a highly localized field which may be neglected in far-zone field calculations.

IX. THE EXCITATION VOLTAGES

From Eq. (12) and reciprocity, the excitation voltages are given by

$$(36) \qquad V_m = \int_m \underline{F}_m \cdot \underline{E}_i \, d\ell$$

where $\underline{E}_i$ denotes the incident field generated by $(\underline{J}_i, \underline{M}_i)$ radiating in the homogeneous medium. The integration extends over both arms or segments of test dipole m.

If the incident field is generated by a distant source with spherical coordinates (r_o,θ_o,ϕ_o),

$$(37) \qquad \underline{E}_i = \underline{E}_o \exp(\gamma\, \underline{r}\cdot\hat{r}_o)$$

where $\underline{E}_o$ is a vector constant, $\hat{r}_o$ is a unit vector from the coordinate origin to the distant source, and $\underline{r}$ is the radial vector from the origin to the observation point. From Eqs. (36) and (37), the excitation voltages induced by an incident plane wave are

$$(38) \qquad V_m = \int_m \underline{F}_m\cdot\underline{E}_o \exp(\gamma\, \underline{r}\cdot\hat{r}_o)\, d\ell$$

Now consider the field $\underline{E}_m$ generated by test dipole m when radiating in the homogeneous medium. Using the vector potential, we find the field at the distant point (r_o,θ_o,ϕ_o) to be

$$(39) \qquad \underline{E}_m = -\frac{s\mu\, e^{-\gamma r_o}}{4\pi r_o} \int_m \underline{F}_m \exp(\gamma\, \underline{r}\cdot\hat{r}_o)\, d\ell$$

where the radial component is to be suppressed. From Eqs. (38) and (39),

$$(40) \qquad V_m = -\frac{4\pi r_o}{s\mu}\, e^{\gamma r_o}\, \underline{E}_o\cdot\underline{E}_m$$

Equations (38) and (40) are useful in plane-wave scattering problems. If the source $(\underline{J}_i,\underline{M}_i)$ is near the wire structure, we have a near-zone scattering problem and employ Eq. (36)

A wire structure is usually called a scatterer if the source $(\underline{J}_i,\underline{M}_i)$ is located some distance away, and an antenna if the source is at the wire surface. In electromagnetic theory, however, there is no fundamental distinction between the scattering problem and the antenna problem. The antenna problem is merely an extreme example of near-zone scattering.

If an antenna is fed with a parallel-wire transmission line, the transmission line is properly considered to be part of the radiating system. In addition to the TEM mode, higher-order modes will exist on the transmission line. Thus, moment methods are employed to determine the current distribution on the transmission line as well as on the antenna. If a wire antenna is fed through a coaxial cable, the source may be modeled as a magnetic surface-current density $\underline{M}_i$ on the aperture surface of the coaxial feed. The shape of the source $\underline{M}_i$ is determined by the details of the terminal region. Thus, a voltage generator may be modeled as a magnetic disk or a magnetic tube as indicated by Otto[18] in 1968.

Consider a wire antenna driven by a voltage generator v_i located at one of the current sampling points ℓ_i. The generator voltage v_i is

considered positive if it tends to force a current in the direction of the expansion mode $\underline{F}_i(\ell)$. From Eqs. (12) and (36), the excitation voltages are

$$(41) \qquad V_m = \int_m \underline{F}_m \cdot \underline{E}_i \, d\ell = - \iint \underline{M}_i \cdot \underline{H}^m \, ds$$

where the line integral extends over test dipole m and the surface integral extends over the magnetic source $\underline{M}_i$. If the magnetic source is approximated by a loop encircling the wire and M_i is uniform around the loop, then

$$(42) \qquad \underline{M}_i = - \hat{\phi} \, v_i$$

If the loop has small radius b, Eq. (41) reduces to

$$(43) \qquad V_m = b \, v_i \oint_i \hat{\phi} \cdot \underline{H}^m \, d\phi.$$

If displacement currents are neglected, Eq. (43) and Ampere's law yield

$$(44) \qquad V_m = v_i \, F_m(\ell_i)$$

From Eq. (44), all the excitation voltages V_m vanish except one: $V_i = v_i$. Although this simple result is often adequate, the accuracy and convergence of the solution may be improved by modeling the source as a magnetic disk or tube (instead of a loop) and using Eq. (41). The approximate result in Eq. (44) may be regarded as the delta-gap model.

Now consider a wire antenna fed with a coaxial cable with inner and outer radii a and b, and let the inner conductor extend to form part of the antenna with radius a. If the antenna is fed through a large ground plane, image theory may be employed. In this case, all the wire segments may have the same radius a. Otherwise the coaxial cable must be considered to be part of the radiating system, and some of the segments of the wire antenna will have radius a and others will have radius b. In either case, the source may be modeled as an annular disk of magnetic current with inner and outer radii a and b. The magnetic surface current density will not be uniform over the disk, and a suitable approximation is

$$(45) \qquad \underline{M}_i = \frac{-\hat{\phi} \; v_i}{\rho \, \ell n \, (b/a)}$$

where ρ denotes the radial distance from the axis of the disk and v_i is the TEM-mode voltage in the coaxial cable.

From Eqs. (41) and (45), it is noted that the excitation voltages differ from the generator voltages except in the delta-gap approximation. The relation has the form:

$$(46) \qquad V_m = \sum_{n=1}^{N} S_{mn} v_n$$

The complex quantities S_{mn} are determined via Eqs. (41) and (with magnetic disks) (45). Thus, the wire antenna has one set of terminal currents and two sets of terminal voltages. The port voltages v_m are related to the port currents I_m by

$$(47) \qquad v_m = \sum_{n=1}^{N} z_{mn} I_n$$

The open-circuit port impedance matrix z_{mn} must be symmetric if the media are reciprocal. The moment (or excitation) voltages are related to the moment currents by

$$(48) \qquad V_m = \sum_{n=1}^{N} Z_{mn} I_n$$

The open-circuit moment impedance matrix Z_{mn} need not be symmetric. In antenna theory and applications, the port voltages and impedances are of basic importance but the moment voltages and impedances are useful only as a means for calculating the port parameters. The transformation from Z_{mn} to z_{mn} is determined by Eq. (46).

If the test sources were the same as the expansion modes, the moment voltages V_m and impedances Z_{mn} would be the same as the port voltages v_m and impedances z_{mn}.

X. RADIATION EFFICIENCY

In this section the frequency is considered real. That is, $s = j\omega$ and ω is real. Furthermore, let $\underline{E}$ and $\underline{H}$ denote the rms field intensities. Both the wire and the surrounding homogeneous medium may have finite conductivities.

When the wire structure is excited as an antenna, the time-average power input is the sum of the powers delivered at the various ports:

$$(49) \qquad P_i = \text{Real} \sum_{n=1}^{N} v_n I_n^*$$

The time-average power dissipated in the wire antenna is

$$(50) \qquad P_d = \text{Real} \oiint_S (\underline{E} \times \underline{H}^*)\cdot ds = \frac{R_s}{2\pi a} \int_0^L \underline{I}\cdot\underline{I}^* \, d\ell$$

where S denotes the closed surface of the wire, $\underline{ds}$ is directed inward on S, and R_s is the surface resistance. The last form in Eq. (50) is a convenient approximation based on Eqs. (3), (8) and (9).

Suppose the voltage generators are modeled with tubular magnetic current sources with radius slightly larger than that of the wire. The wire need not have any gaps at the terminals. In calculating the power dissipated in the wire via Eq. (50), we integrate over the wire surface S and consider the magnetic sources $\underline{M}_i$ to be outside S. The time-average power radiated from the antenna to the exterior region is

$$(51) \qquad P_r = \text{Real} \oiint_{S'} (\underline{E} \times \underline{H}^*)\cdot \underline{ds}$$

where surface S' lies just outside surface S so the magnetic sources $\underline{M}_i$ are in the interior region of S'. From Eqs. (49), (50) and (51) and Poynting's theorem,

$$(52) \qquad P_i = P_d + P_r \quad .$$

If the ambient medium has finite conductivity, the "radiated power" P_r is actually dissipated in the exterior region. The radiation efficiency may be defined as the ratio of the power radiated to the power input:

$$(53) \qquad E_r = P_r/P_i \quad .$$

If Eq. (53) is employed, the antenna will have perfect efficiency unless it is constructed of dissipative media.

An alternative definition has been proposed by Tsao[19] as follows. It is reasonable to consider a certain portion of the exterior-region dissipation to be a propagation phenomenon rather than intrinsically an antenna problem. Therefore, let the time-average power radiated by the antena be defined as follows:

$$(54) \qquad P_R = e^{2\alpha r} \, \text{Real} \oiint (\underline{E} \times \underline{H}^*) \cdot \underline{ds}$$

where $\gamma = \alpha + j\beta$ and the integration covers a spherical surface with radius r centered at the antenna. With this definition, the radiated power is independent of the range r in the far-zone region. Now the radiation efficiency is defined by

$$(55) \qquad E_R = P_R/P_i$$

The definition in Eq. (55) penalizes the antenna not only for power dissipated in the antenna structure but also for excess near-zone losses. Thus, even a perfectly conducting antenna may have imperfect efficiency. Furthermore, two antennas (a small loop and a small dipole) may have the same distant fields (except for polarization) but different near-zone fields. They will generally have different near-zone losses, input powers and radiation efficiencies according to Eq. (55). The antenna with higher efficiency will be preferred except perhaps in near-zone applications.

Equations (54) and (55) are based on the idea that the normal propagation losses in the medium will introduce an attenuation factor $e^{-\alpha r}$ in the fields. This attenuation disappears if the medium is lossless. If the near-zone losses for a particular antenna exceed this amount, this antenna will have less than perfect efficiency. Similarly, if the near-zone losses are smaller than the normal propagation losses, the antenna efficiency may exceed 100 per cent. This situation may arise with a large spherical antenna if the interior of the sphere is lossless and the range r in Eq. (54) is measured from the center of the sphere.

For a given antenna, the near-zone losses and attenuation generally increase as the conductivity of the medium is increased. In some cases, however, the time-average power radiated P_R will increase with increasing conductivity of the medium. This occurs when the actual near-zone attenuation is a slowly varying function of the conductivity and is over-compensated by the factor $e^{2\alpha r}$ in Eq. (54).

For an antenna in a conducting medium, the directive gain is defined as follows:

$$(56) \qquad G_d = \frac{\text{power density at the point } (r,\theta,\phi)}{\text{average power density on the sphere of radius } r}$$

In the far zone, the directive gain is independent of the range r and

$$(57) \qquad G_d = \frac{4\pi \, \underline{F} \cdot \underline{F}^*}{\oint\!\!\oint \underline{F} \cdot \underline{F}^* \sin\theta \, d\theta \, d\phi}$$

where $\underline{F}$ is defined by

$$(58) \qquad \underline{E} = \underline{F}(\theta,\phi) \, \frac{e^{-\gamma r}}{r}$$

The power gain may be defined as follows [19]:

$$(59) \qquad G_p(r,\theta,\phi) = 4\pi r^2 e^{2\alpha r} S(r,\theta,\phi)/P_i$$

where P_i denotes the time-average power input and $S(r,\theta,\phi)$ is the time-average power density at the observation point.

XI. FORWARD SCATTERING THEOREM

Let a time-harmonic plane wave propagate through a homogeneous conducting medium (μ_0,ε_0) and illuminate an inhomogeneous conducting target (μ,ε). The frequency is considered real, and $\underline{E}$ and $\underline{H}$ denote the rms field intensities.

To simplify the discussion, let the target and the medium have the same real permeability μ_0. Let ε_0 and ε denote the complex permittivity of the medium and the target, respectively. The parameters μ_0 and ε_0 should not be confused with those of free space

Let $(\underline{E}_i,\underline{H}_i)$ denote the incident plane-wave field, $(\underline{E}_s,\underline{H}_s)$ the scattered field and $(\underline{E},\underline{H})$ the total field. In 1953, Rhodes[20] used Maxwell's equations to demonstrate that the scattered field may be generated by the equivalent electric current density

$$(60) \qquad \underline{J}_{eq} = j\omega(\varepsilon - \varepsilon_0)\,\underline{E}$$

radiating in the ambient medium (μ_0,ε_0). Using the vector potential and the "volume equivalence theorem" of Rhodes, we find the far-zone scattered field as follows:

$$(61) \qquad \underline{E}_s = \frac{-j\omega\mu_0 e^{-\gamma r}}{4\pi r} \iiint_V \underline{J}_{eq} \exp(\gamma\, \underline{r}'\cdot\hat{r}_s)\, dv'$$

where $\gamma = j\omega\sqrt{\mu_0\varepsilon_0}$, $\underline{r}'$ is a vector from the origin to the source-point, $\hat{r}_s$ is a unit vector from the origin toward the distant observation point, and V denotes the volumetric interior region of the target.

Let P denote the "total time-average power" defined as follows:

$$(62) \qquad P = \text{Real} \iiint_V \underline{J}_{eq} \cdot \underline{E}_i^* \, dv$$

In the forward-scattering situation, the incident plane wave travels in the direction of $\hat{r}_s$ and

(63) $$\underline{E}_i = \underline{E}_o \exp(-\gamma \underline{r} \cdot \hat{r}_s)$$

(64) $$P = \text{Real} \iiint_V \underline{J}_{eq} \cdot \underline{E}_o^* \exp[(-\alpha + j\beta)\, \underline{r} \cdot \hat{r}_s]\, dv.$$

From Eq. (61)

(65) $$\underline{E}_s \cdot \underline{E}_o^* = \frac{-j\omega\mu_o\, e^{-\gamma r}}{4\pi r} \iiint_V \underline{J}_{eq} \cdot \underline{E}_o^* \exp[(\alpha + j\beta)\, \underline{r}' \cdot \hat{r}_s]\, dv'$$

The integrals in Eqs. (64) and (65) are identical except for a minus sign. Therefore, we define a "modified forward-scattered field" $\underline{E}_s^m$ as in Eq. (65) but with α replaced by $(-\alpha)$ in the integrand. Thus, the total time-average power is related to the modified forward-scattered field as follows:

(66) $$P = \text{Real} \left[j \frac{4\pi r\, e^{\gamma r}}{\omega\, \mu_o} \underline{E}_s^m \cdot \underline{E}_o^* \right]$$

Equation (66) states the forward scattering theorem for a target in a homogeneous conducting medium. If the medium is lossless, α vanishes and $\underline{E}_s^m$ can be replaced with $\underline{E}_s$. Thus, Eq. (66) reduces correctly to the well-known theorem for a target in a lossless medium where P denotes the time-average power extracted from the incident plane wave. That is, P is the sum of the time-average power dissipated in the target and the time-average power scattered by the target.

Since $\underline{E}_i = \underline{E} - \underline{E}_s$ Eq. (62) yields:

(67) $$P = P_d + P_s$$

where

(68) $$P_d = \text{Real} \iiint_V \underline{J}_{eq} \cdot \underline{E}^*\, dv$$

(69) $$P_s = -\,\text{Real} \iiint_V \underline{J}_{eq} \cdot \underline{E}_s^*\, dv$$

From Poynting's theorem, Eq. (69) seems reasonable as a definition of the time-average scattered power. When radiating in the homogeneous medium (μ_o, ε_o) with the incident plane wave removed, $\underline{J}_{eq}$ is the source of the scattered field.

From Eqs. (60) and (68),

$$(70) \qquad P_d = \iiint_V \sigma \, \underline{E}\cdot\underline{E}^* \, dv - \sigma_o \iiint_V \underline{E}\cdot\underline{E}^* \, dv$$

where σ and σ_o denote the conductivities of the target and the medium, respectively. The first integral in Eq. (70) is clearly the time-average power dissipated in the target. The last integral is not so easy to interpret, but the integrand may be expanded as follows:

$$(71) \qquad \underline{E}\cdot\underline{E}^* = \underline{E}_i\cdot\underline{E}_i^* + \underline{E}_s\cdot\underline{E}_s^* + \underline{E}_i\cdot\underline{E}_s^* + \underline{E}_s\cdot\underline{E}_i^*$$

From the last term in Eq. (70) and the first two terms in Eq. (71), the time-average power budget must account for the power dissipated by the incident plane wave and the scattered field, respectively, in region V with homogeneous medium (μ_o, ε_o). No interpretation is offered for the last two terms in Eq. (71), but their sum is real.

The last term in Eq. (70) vanishes if the ambient medium is lossless, and it may be negligible if the target conductivity greatly exceeds the conductivity of the medium. In these cases, the total power P is simply the sum of the power dissipated in the target and the power scattered by the target.

For a target in a conducting medium, the forward-scattering theorem does not appear to be useful for experimental measurements because the modified scattered field $\underline{E}_s^m$ is not available. This quantity is calculable, however, so the theorem may find application in the computation of extinction cross sections.

For a target in a homogeneous conducting medium, it is convenient to define the radar cross section (or echo area) as follows:

$$(72) \qquad \sigma = \lim_{r\to\infty} \; 4\pi r^2 \, e^{2\alpha r} \; S_s/S_i$$

where S_s and S_i denote the time-average power densities in the scattered and incident fields, respectively. When echo-area data are presented for a specific target, it is necessary to specify the location of the point in space where S_i is evaluated and from which the range r is measured. Equation (72) reduces to the standard definition for a target in a lossless medium as the attenuation constant α tends to zero. Without the factor $e^{2\alpha r}$, the echo area would vanish for every finite target in a conducting medium.

The factor $e^{2\alpha r}$ in Eq. (72) compensates for the normal attenuation of the outward-traveling scattered wave. Because of this factor, a low-loss dielectric sphere may have a large echo area when immersed in a conducting medium. If the range r is measured from the center of the sphere, Eq. (72) allows for attenuation starting from the center whereas the actual attenuation begins at the surface of the target. For a given target, the near-zone losses in the scattered field will generally increase as the conductivity of the medium is increased. In some cases the near-zone attenuation will increase more slowly than the "normal rate", the exponential factor in Eq. (72) will overcompensate, and the echo area will increase with increasing conductivity of the medium. This phenomenon is closely related to that previously discussed for the radiation efficiency as defined in Eq. (55).

The absorption cross section is defined by the ratio of the time-average power absorbed (dissipated) in the target and the time-average power density of the incident plane wave. The scattering cross section is the ratio of the time-average power scattered and the time-average power density of the incident wave. The extinction cross section is the sum of the absorption and scattering cross sections. If the scattered power is defined by Eq. (69), these cross-section definitions are suitable even for a target in a conducting medium.

Now let us consider briefly the scattering problem for a thin-wire structure with conductivity much greater than that of the ambient medium. Suppose we have already calculated the current distribution $I(\ell)$ induced on the wire by an incident plane wave. The same current distribution may be induced by a set of equivalent port-voltage generators V_n inserted at the various ports along the wire, and these voltages are readily calculated. Let P_i denote the time-average power input to the wire system as defined by Eq. (49). This power input must be the sum of the power dissipated in the wire and the power radiated or scattered from the wire. The power dissipated is readily calculated via Eq. (50), and the power input from Eq. (49). Finally, the scattered power is obtained from $P_i - P_d$. Dividing by the incident power density, we obtain the absorption, scattering and extinction cross sections.

XII. NUMERICAL RESULTS

In comparison with antennas and scatterers in free space, relatively little data are available for structures in a conducting medium. Therefore, it is not necessary or desirable to choose a complicated configuration to illustrate trends. Figure 3 illustrates the backscatter echo area of a perfectly conducting straight wire for broadside incidence with Eq. (72). For defining the range r and the incident power density S_i, the coordinate origin is located at the center of the wire. At the highest frequency (100 MHz), the wire length is approximately equal to the wavelength in the ambient medium. As the conductivity of the medium increases, the echo area decreases at first and then increases. This is

not surprising, in view of the discussion following Eq. (72). It seems reasonable that the highly resonant properties of the thin straight wire should decrease and finally disappear. All the numerical results presented in this section were calculated with the sinusoidal reaction technique. For these calculations, the wire was divided into a number J of segments where J = 6 or

(73) $$J = 3.2\,|\gamma h|$$

(whichever is larger) where h denotes the half-length of the wire.

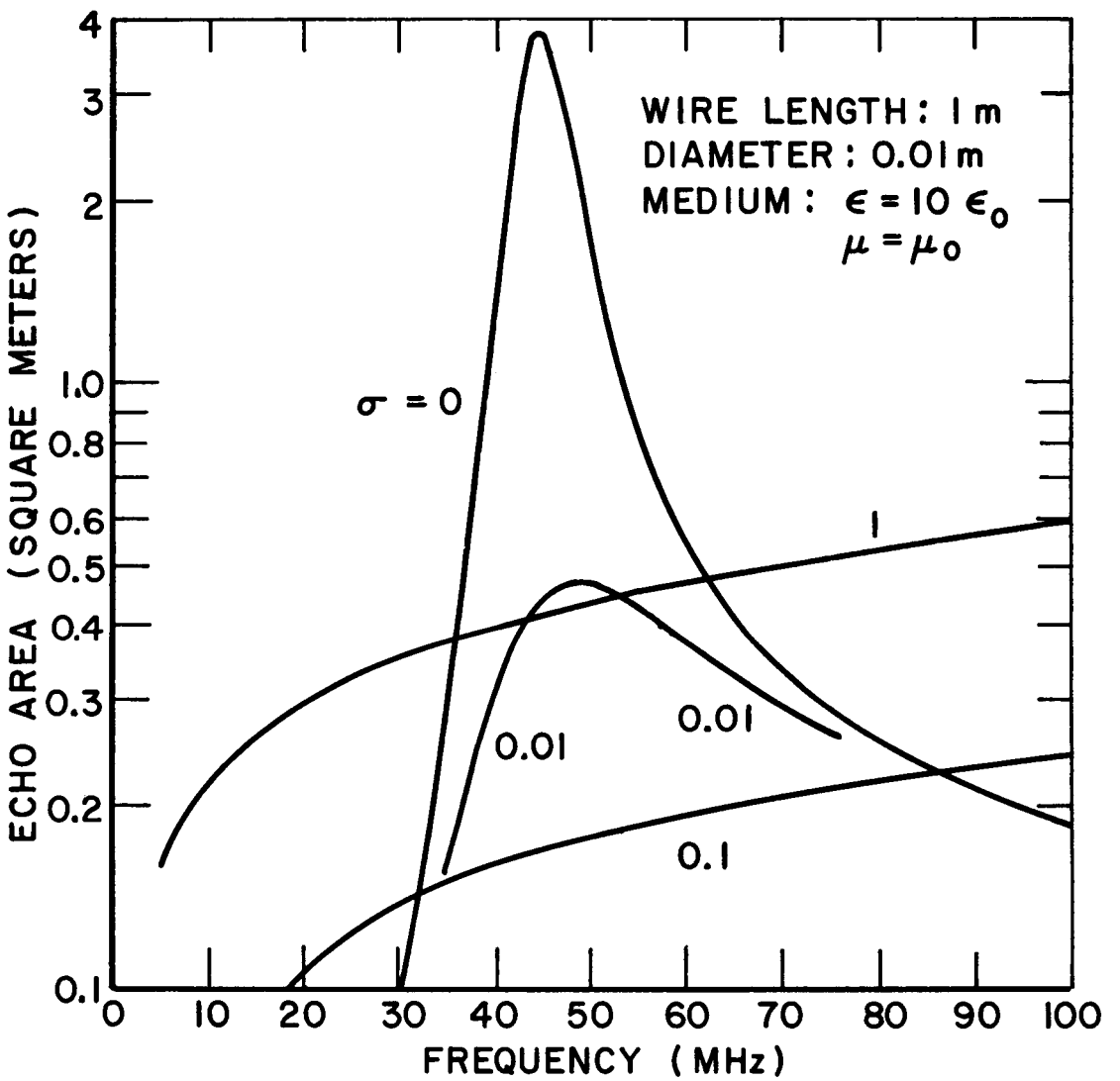

Fig. 3. Broadside backscatter for uninsulated perfectly-conducting straight wire in homogeneous medium with conductivity σ in mhos/m.

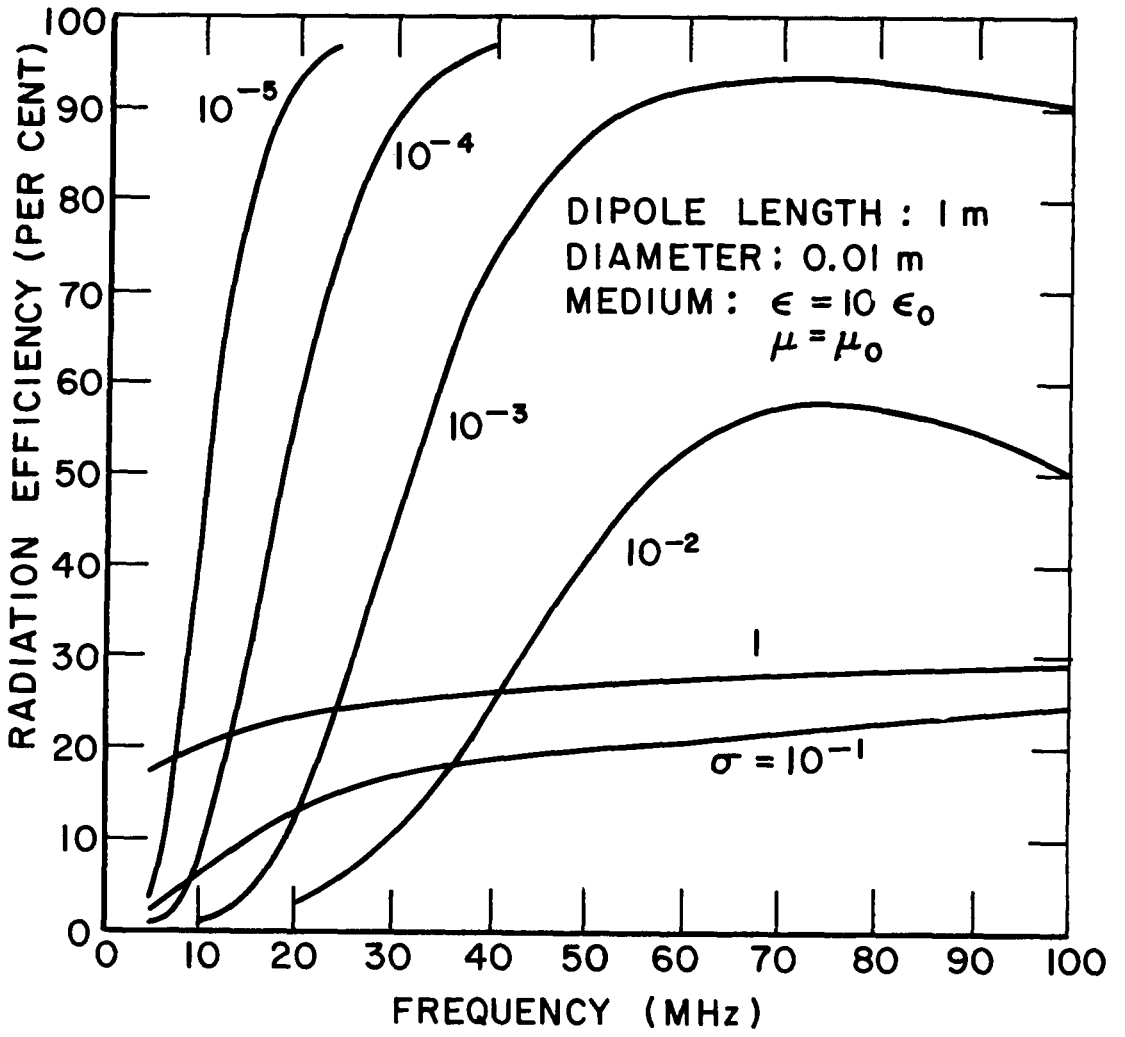

Fig. 4. Radiation efficiency of uninsulated perfectly-conducting center-fed linear dipole in a homogeneous medium with conductivity σ in mhos/m.

Figure 4 illustrates the radiation efficiency of a perfectly-conducting center-fed linear dipole as defined by Eq. (55). The radiated power was calculated via Eq. (54) by integrating the power density over a far-zone sphere. Again, the center of the wire was selected as the coordinate origin for measuring the range r. The power input was obtained from the terminal current and voltage. The low efficiency observed in the low-frequency range is attributed to the excess near-zone losses of the short uninsulated dipole. As the conductivity of the medium increases, the efficiency decreases at first and then increases. This is not surprising in view of the discussion following Eq. (55).

Figures 5 and 6 show the resistance and reactance of the center-fed linear dipole mentioned above.

Before we introduce the next figure, it is necessary to define some terms. In common language, a tripod is a figure with three straight legs intersecting at a common junction. Thus, it is reasonable to define a quadripod as a figure with four straight legs (or arms) intersecting at a common junction. By analogy with the regular tetrahedron or a regular polygon, the regular quadripod has four arms and each arm has the same length h. Furthermore, each arm makes the same angle of 109.5 degrees with each of the other arms. The regular quadripod is a nonplanar structure.

Figure 7 illustrates five poles of the admittance of a perfectly-conducting regular quadripod, plotted on the complex γh plane. These poles are invariant with respect to the location of the terminals on the thin-wire structure, although some of the poles will not be observed if the terminals are located at the junction. These admittance poles are also the poles of the scattering function for near-zone or far-zone scattering, and they are independent of the incidence direction.

For a perfectly conducting structure, scaling theory indicates that the poles may be presented without specifying the frequency or the parameters of the ambient medium. The fundamental quantity γh is dimensionless, and it does not matter whether the complex values of γ result from a complex ambient medium or the choice of a complex frequency. Thus, Fig. 7 may be interpreted as the complex frequency plane or the complex medium plane, but the range of validity is more general than either. Some of the quadripod poles in Fig. 7 are the same as those of a simple bent wire (the V antenna) with an angle of 109.5 degrees.

For an imperfectly conducting target, scaling is much more restrictive. For example, one might plot the poles of a copper wire immersed in sea water. These poles might be plotted on the complex frequency plane, and it would be necessary to specify the ambient medium and the target medium. In calculating these poles, one must have experimental or theoretical data for the complex permittivity of both media at complex frequencies.

Figures 8 and 9 show the radiation efficiency of a dipole and a loop in free space as a function of the wire conductivity. Finally, Figs. 10 and 11 illustrate the conductance and susceptance of bare and insulated dipoles in free space.

Although experimental confirmation is not available for the numerical results presented here, the examples concern antennas and scatterers with simple shapes to encourage others to compare with their calculations or measurements. The numerical results were obtained with a computer program that has been tested extensively with many antennas and targets in free space. Pole plots obtained with this program show excellent agreement with those of Tesche[21] for a straight wire. The program has been employed to analyze the transmission of short pulses between coupled bow-tie antennas buried in the earth, with excellent experimental verification. For a linear dipole immersed in a salt water solution, our admittance and impedance calculations show close

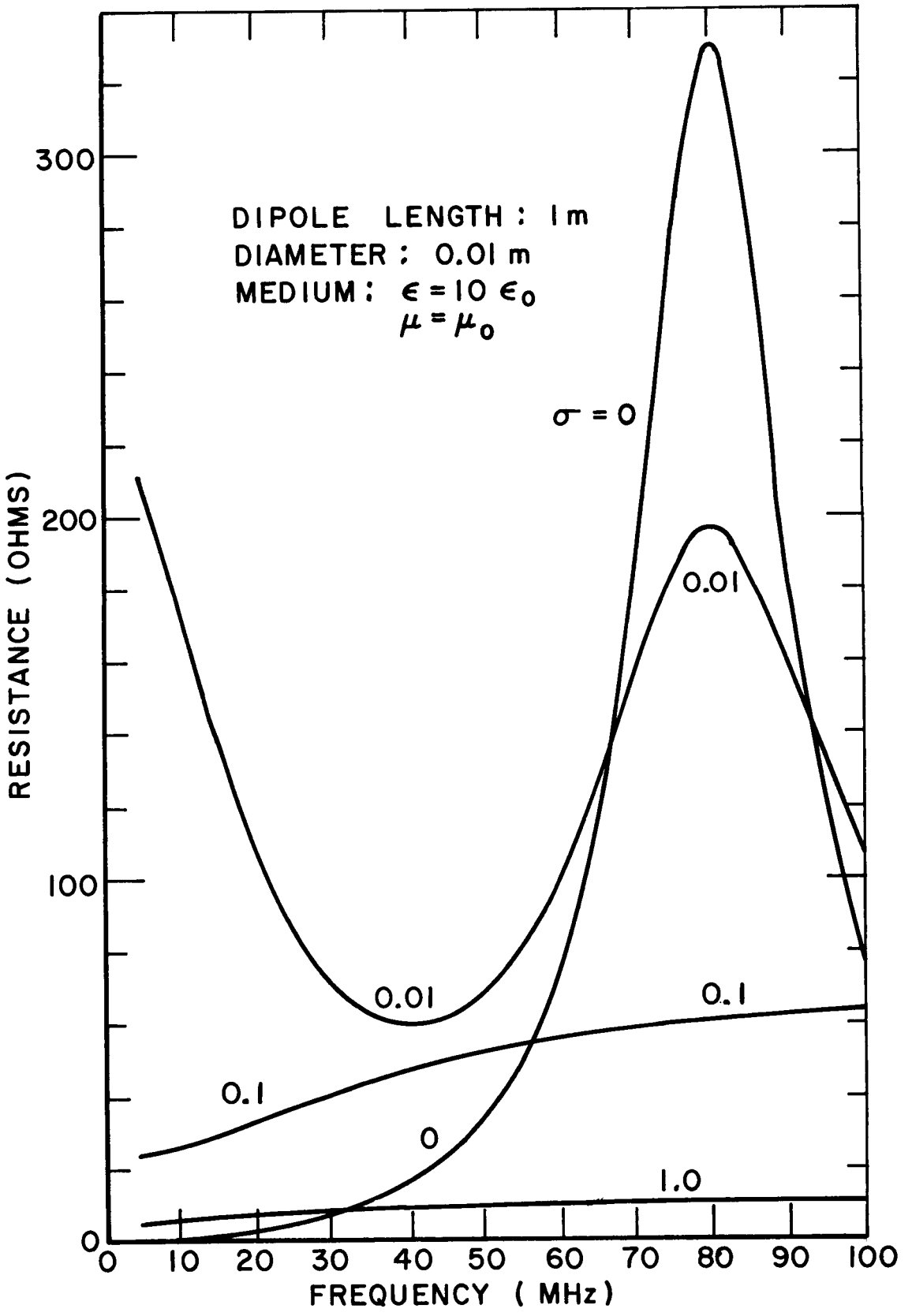

Fig. 5. Resistance of uninsulated perfectly-conducting center-fed linear dipole in a homogeneous medium with conductivity σ in mhos/m.

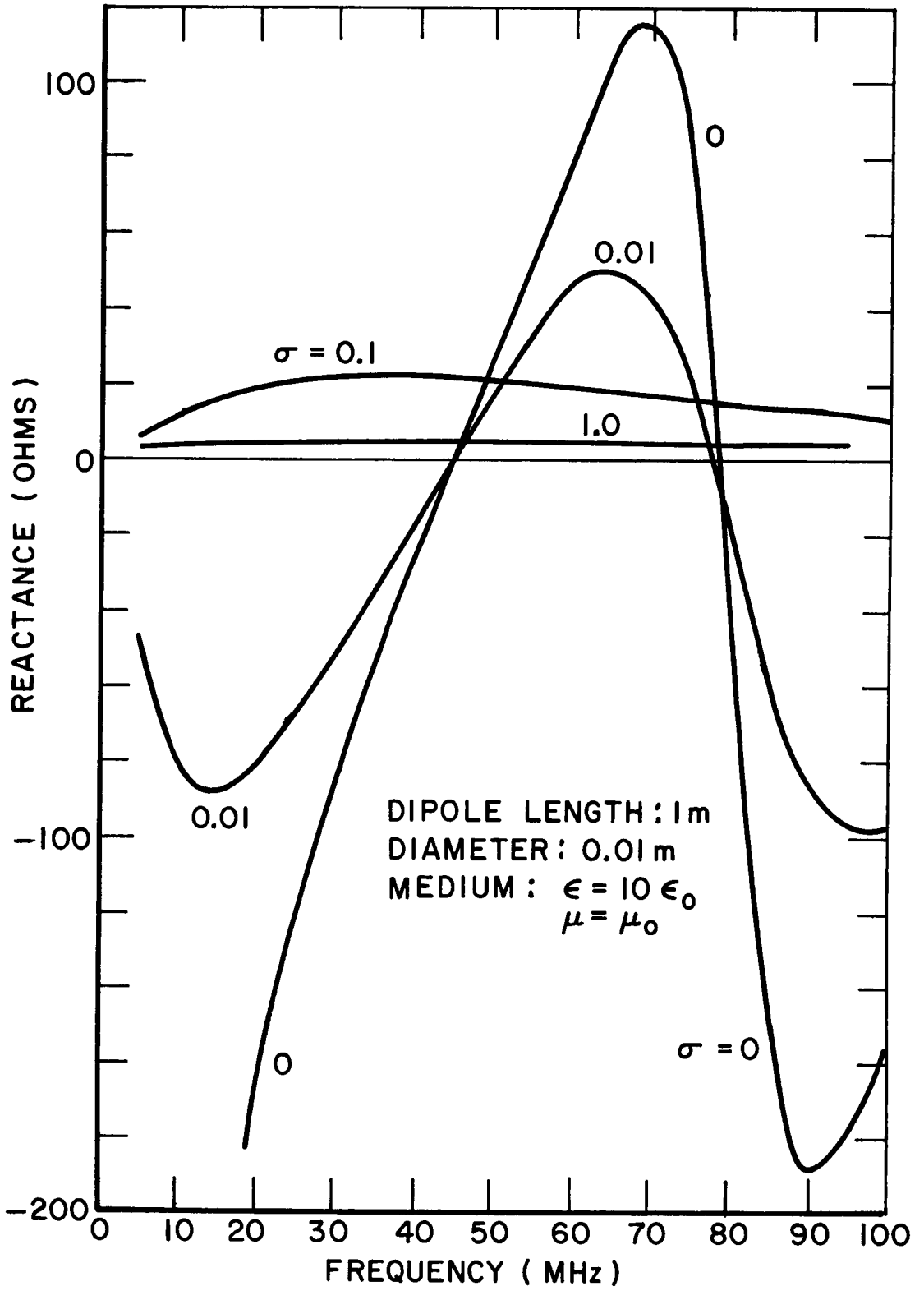

Fig. 6. Reactance of uninsulated perfectly-conducting center-fed linear dipole in a homogeneous medium with conductivity σ in mhos/m.

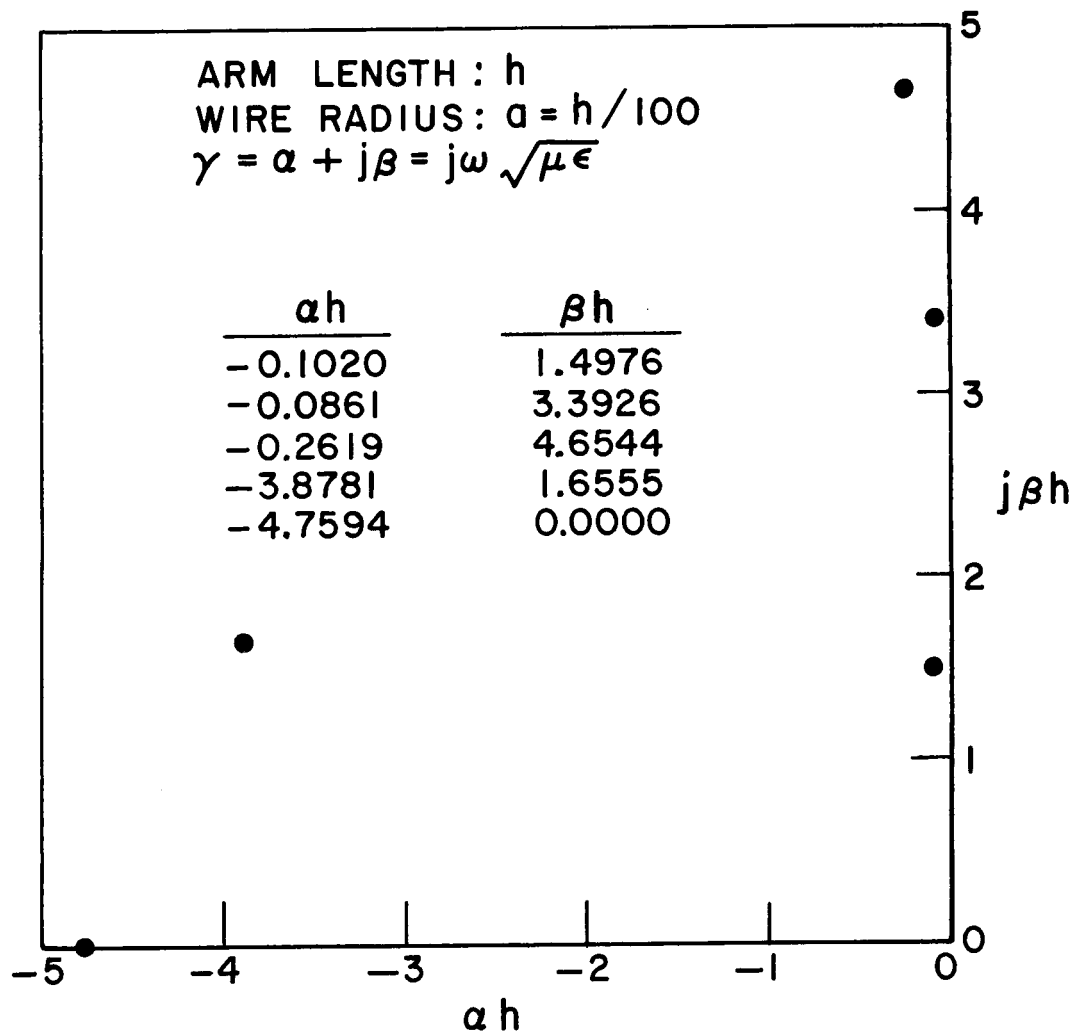

Fig. 7. Calculated poles of the admittance of a perfectly-conducting regular quadripod, plotted on the complex γh plane.

agreement with measurements by Iizuka and King[22] and Siegel and King[23] when γa is less than 0.07 and the dipole length exceeds the wire diameter by a factor of at least 30. This justifies confidence in the formulation, the computer program and the numerical results.

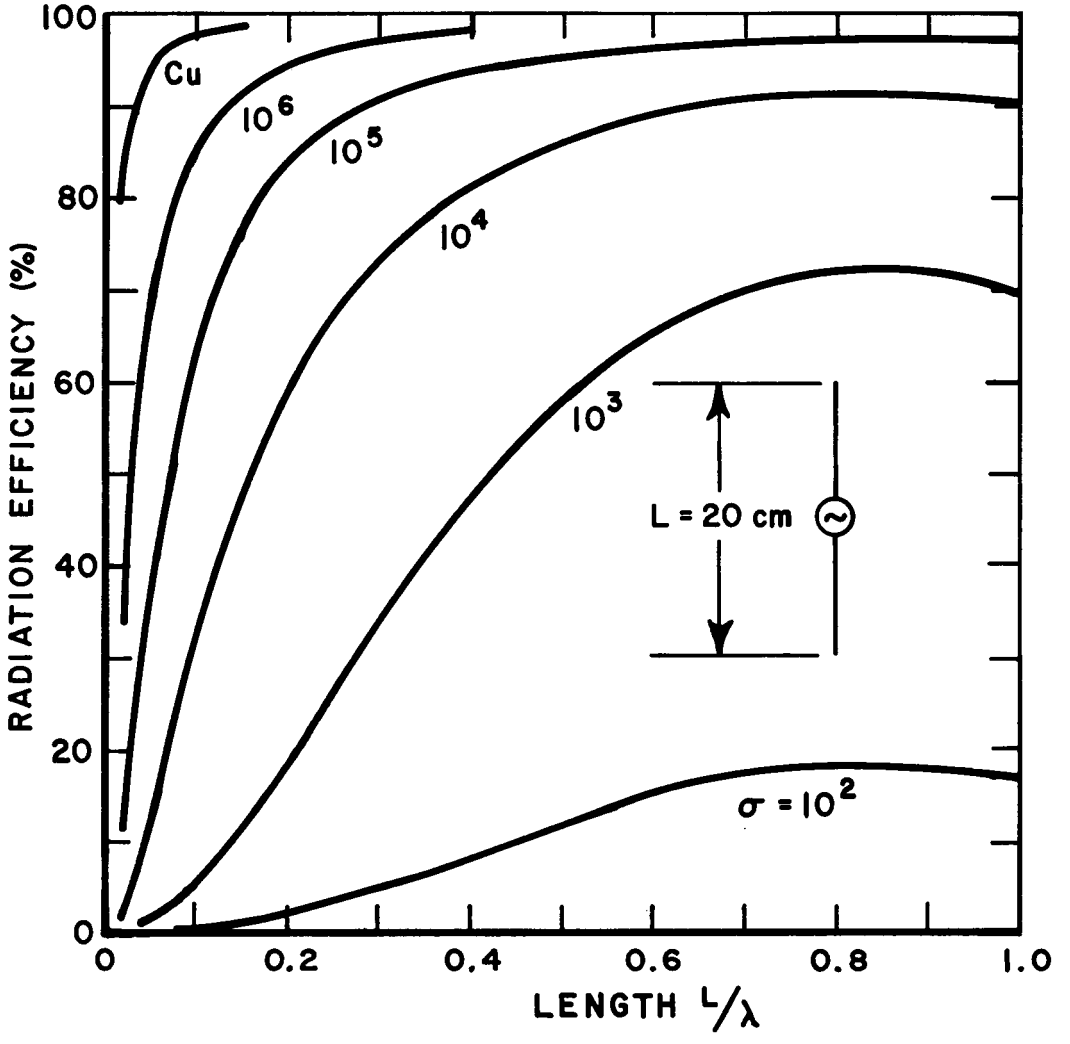

Fig. 8. Radiation efficiency of center-fed dipole in free space. The parameter is the conductivity in mhos per meter. Wire diameter: 1/16 inch solid.

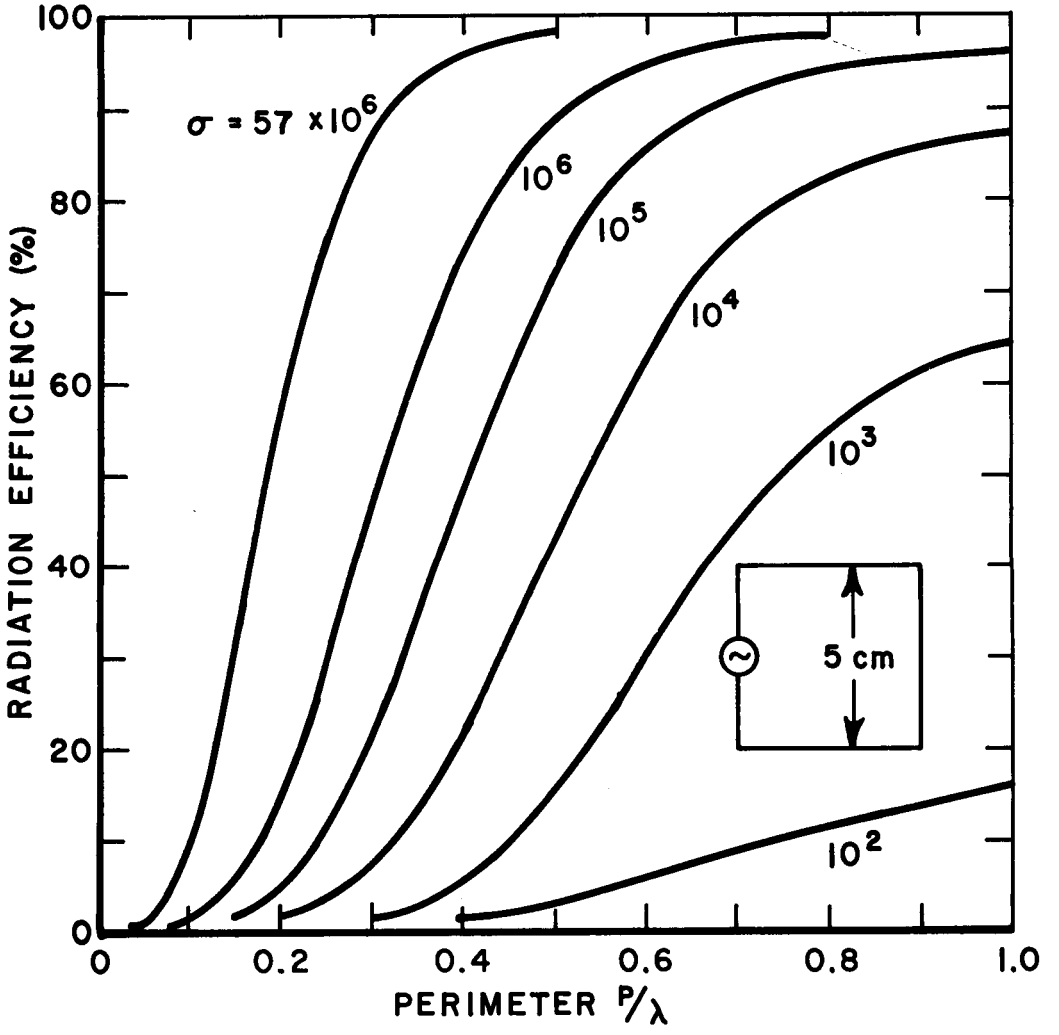

Fig. 9. Radiation efficiency of square loop antenna in free space. The parameter is the conductivity in mhos per meter. Wire diameter: 1/16 inch solid.

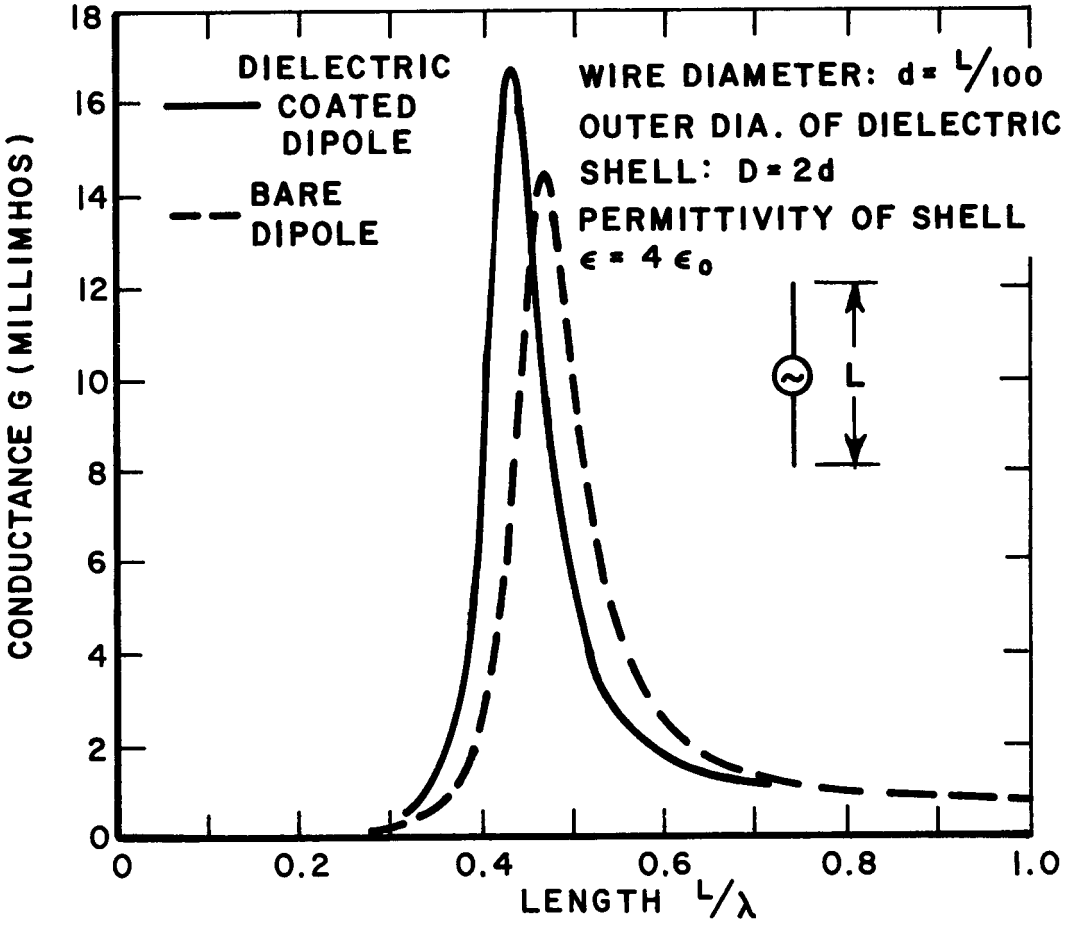

Fig. 10. Conductance of perfectly-conducting center-fed dipole in free space.

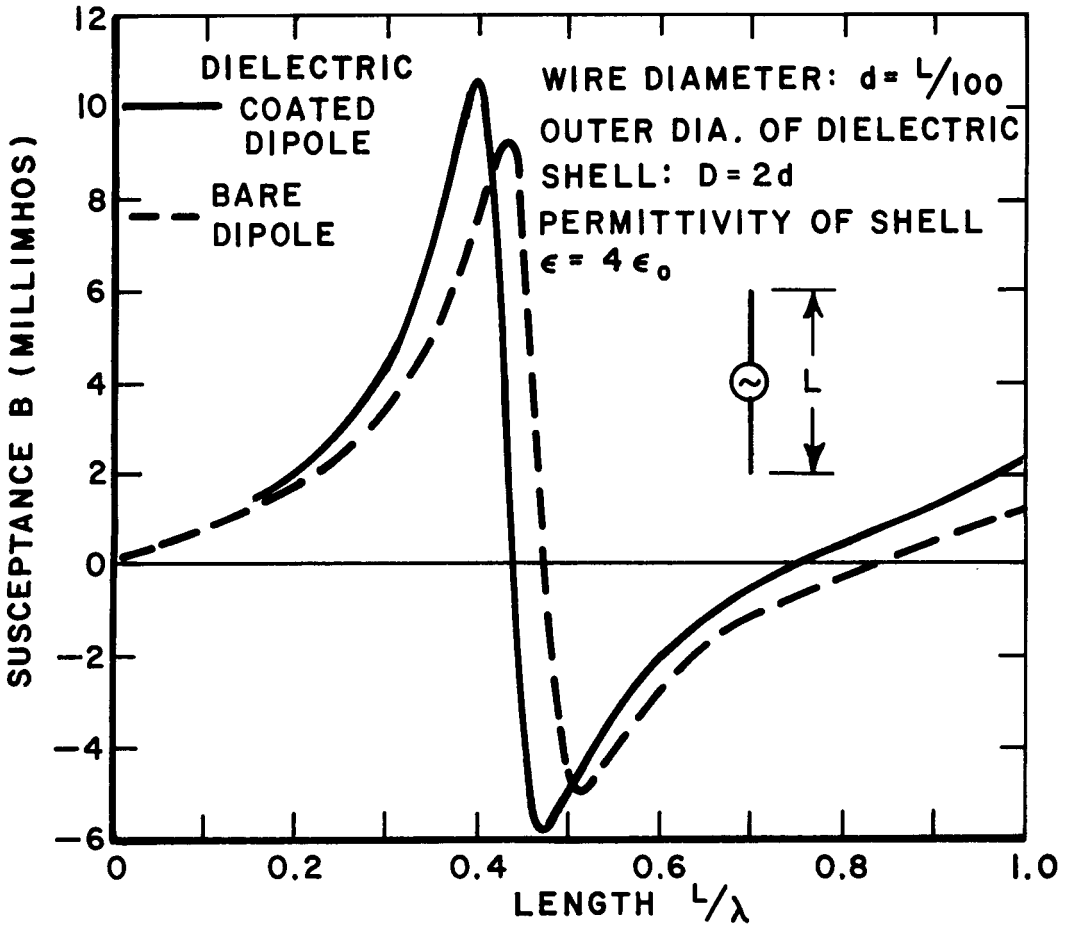

Fig. 11. Susceptance of perfectly-conducting center-fed dipole in free space.

XIII. SUMMARY

Rumsey's reaction integral equation is discussed, and it is pointed out that it is more general than the electric field integral equation or the magnetic field integral equation. The forward scattering theorem is developed for an arbitrary target in homogeneous conducting medium.

The sinusoidal reaction formulation is presented for an arbitrary thin-wire structure in a conducting medium. The wire structure may have finite conductivity and lumped loading, and some portions of the wire may be insulated and others bare. The analysis is performed in the real or complex frequency domain, and it covers both the antenna and the scattering situations. A fundamental distinction is indicated between the moment voltages and impedances and the multiport voltages and impedances.

Numerical results are included to illustrate the backscattering properties of a straight wire as a function of the frequency and the conductivity of the medium. Similar graphs illustrate the radiation efficiency and impedance of a center-fed linear dipole. Several poles are plotted on the complex γh plane for the admittance function of a "regular quadripod". Appendices present the near-zone and far-zone fields of a sinusoidal electric monopole in a conducting medium.

REFERENCES

1. Carter, P.S., "Circuit Relations in Radiating Systems and Applications to Antenna Problems," IRE Proc., Vol. 20, (June 1932), pp. 1004-1041.

2. King, H.E., "Mutual Impedance of Unequal Length Antennas in Echelon," IRE Trans., Vol. AP-5, (July 1957), pp. 306-313.

3. Baker, H.C. and A.H. LaGrone, "Digital Computation of the Mutual Impedance Between Thin Dipoles," IRE Trans., Vol. AP-10, (March 1962), pp. 172-178.

4. Yeh, Y.S. and K.K. Mei, "Theory of Conical Equiangular-Spiral Antennas, Part I - Numerical Technique," IEEE Trans., Vol. AP-15, (September 1967), pp. 634-639.

5. Tanner, R.L. and M.G. Andreasen, "Numerical Solution of Electromagnetic Problems," IEEE Spectrum, (September 1967), pp. 53-61.

6. Miller, E.K. and J.B. Morton, "The RCS of a Metal Plate with a Resonant Slot," IEEE Trans., Vol. AP-18, (March 1970), pp. 290-292.

7. Chao, H.H. and B.J. Strait, "Radiation and Scattering by Configurations of Bent Wires With Junctions," IEEE Trans., Vol. AP-19, (September 1971), pp. 701-702.

8. Richmond, J.H., "Theoretical Study of V Antenna Characteristics for the ATS-E Radio Astronomy Experiment," Report 2619-1, 13 February 1969, The Ohio State University ElectroScience Laboratory, Department of Electrical Engineering; prepared under Contract NAS5-11543 for National Aeronautics and Space Administration, Goddard Space Flight Center, Greenbelt, Maryland. (N69-19062)

9. Richmond, J.H., "Computer Analysis of Three-Dimensional Wire Antennas," Report 2708-4, 22 December 1969, The Ohio State University ElectroScience Laboratory, Department of Electrical Engineering; prepared under Contract DAAD05-69-C-0031 for Department of the Army, Ballistic Research Laboratory, Aberdeen Proving Ground, Maryland.

10. Richmond, J.H. and N.H. Geary, "Mutual Impedance Between Co-Planar-Skew Dipoles," IEEE Trans., Vol. AP-18, (May 1970), pp. 414-416.

11. Richmond, J.H., "Coupled Linear Antennas With Skew Orientation," IEEE Trans., Vol. AP-18, (September 1970), pp. 694-696.

12. Richmond, J.H., "Admittance Matrix of Coupled V Antennas," IEEE Trans., Vol. AP-18, (November 1970), pp. 820-821.

13. Butler, C.M., "Currents Induced on a Pair of Skew Crossed Wires," IEEE Trans., Vol. AP-20, (November 1972), pp. 731-736.

14. Imbriale, W.A. and P.G. Ingerson, "On Numerical Convergence of Moment Solutions of Moderately Thick Wire Antennas Using Sinusoidal Basis Functions," IEEE Trans., Vol. AP-21, (May 1973), pp. 363-366.

15. Kantorovich, L. and V. Krylov, Approximate Methods of Higher Analysis," New York: Wiley, (1964), Chapter 4.

16. Rumsey, V.H., "Reaction Concept in Electromagnetic Theory," Physical Review, Vol. 94, (June 15, 1954), pp. 1483-1491.

17. Schelkunoff, S.A., "On Diffraction and Radiation of Electromagnetic Waves," Physical Review, Vol. 56, (August 15, 1939).

18. Otto, D.V., "Fourier Transform Method in Cylindrical Antenna Theory," Radio Science, (New Series), Vol. 3, No. 11, (November 1968), pp. 1050-1057.

19. Tsao, C.K.H., "Radiation Resistance of Antennas in Lossy Media," IEEE Trans., Vol. AP-19, (May 1971), pp. 443-444.

20. Rhodes, D.R., "On the Theory of Scattering by Dielectric Bodies," Report 475-1, 1 July 1953, The Ohio State University ElectroScience Laboratory (formerly Antenna Laboratory), Department of Electrical Engineering; prepared under Contract AF 18(600)-19 for Wright Air Development Center, Wright-Patterson Air Force Base, Ohio. (AD-18279)

21. Tesche, F.M., "On the Analysis of Scattering and Antenna Problems Using the Singularity Expansion Technique," IEEE Trans., Vol. AP-21, (January 1973), pp. 53-62.

22. Iizuka, K. and R.W.P. King, "The Dipole Antenna Immersed in a Homogeneous Conducting Medium," IRE Trans., Vol. AP-10, (July 1962), pp. 384-392, Figures 7 and 8.

23. Siegel, M. and R.W.P. King, "Electromagnetic Propagation Between Antennas Submerged in the Ocean," IEEE Trans., Vol. AP-21, (July 1973), pp. 507-513, Figure 4

APPENDIX I
NEAR-ZONE FIELD OF SINUSOIDAL LINE SOURCE

Consider an electric line source located on the z axis with endpoints at z_1 and z_2 as shown in Fig. 12. Two of these "monopoles" can be arranged to form a V dipole. The filamentary V dipole is of interest because it is employed as the test source in the sinusoidal reaction technqiue for thin-wire structures.

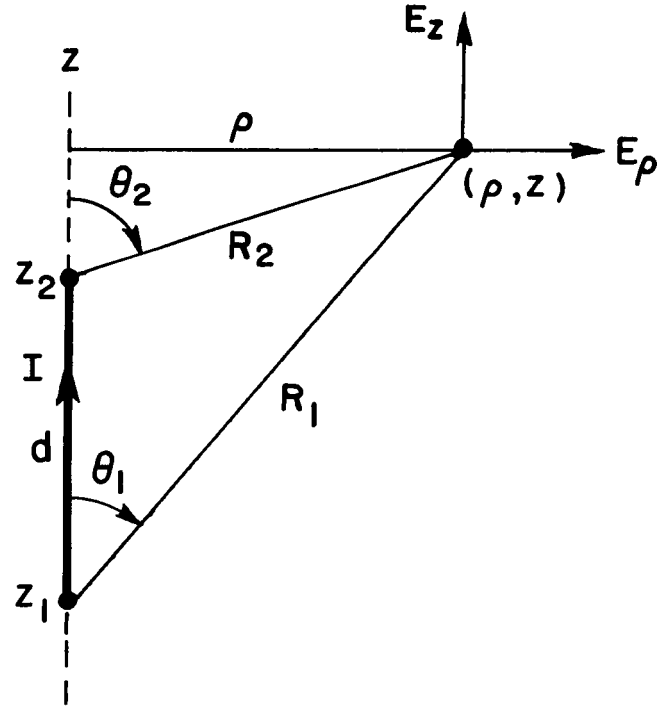

Fig. 12. An electric line source on the z axis and the observation point at (ρ,z).

Let the electric monopole have the following current distribution:

$$I(z) = \frac{I_1 \sinh \gamma(z_2 - z) + I_2 \sinh \gamma(z - z_1)}{\sinh \gamma d} \tag{74}$$

where I_1 and I_2 are the endpoint currents, γ is the complex propagation constant of the medium, $d = z_2 - z_1$ is the source length and the time

dependence e^{st} is understood. The medium is considered to be homogeneous with complex parameters μ and ε. The cylindrical components of the field are $E_\phi = 0$ and

$$(75) \qquad E_\rho = \frac{\eta}{4\pi\rho \sinh \gamma d} \left[(I_1 e^{-\gamma R_1} - I_2 e^{-\gamma R_2}) \sinh \gamma d + (I_1 \cosh \gamma d - I_2) e^{-\gamma R_1} \cos\theta_1 + (I_2 \cosh \gamma d - I_1) e^{-\gamma R_2} \cos\theta_2\right]$$

$$(76) \qquad E_z = \frac{\eta}{4\pi \sinh \gamma d} \left[(I_1 - I_2 \cosh \gamma d) \frac{e^{-\gamma R_2}}{R_2} + (I_2 - I_1 \cosh \gamma d) \frac{e^{-\gamma R_1}}{R_1}\right]$$

$$(77) \qquad \underline{H} = \frac{\hat{\phi}}{4\pi\rho \sinh \gamma d} \left[(I_1 \cos\theta_1 \sinh \gamma d + I_1 \cosh \gamma d - I_2) e^{-\gamma R_1} - (I_2 \cos\theta_2 \sinh \gamma d - I_2 \cosh \gamma d + I_1) e^{-\gamma R_2}\right]$$

where η is the intrinsic impedance of the medium:

$$(78) \qquad \eta = \sqrt{\mu/\varepsilon}$$

These expressions exclude the field contributions from the point charges at the endpoints of the line source, since these charges disappear when two monopoles are connected to form a dipole. For a V dipole, scalar addition applies to the cartesian components (E_x, E_y, E_z) of the field generated by each of the monopoles.

APPENDIX II
FAR-ZONE FIELD OF SINUSOIDAL LINE SOURCE

Consider an electric line source with lendth d and endpoints at (x_1,y_1,z_1) and (x_2,y_2,z_2). The coordinates of any point on the source are

$$x = x_1 + \ell \cos \alpha \tag{79}$$

$$y = y_1 + \ell \cos \beta \tag{80}$$

$$z = z_1 + \ell \cos \gamma \tag{81}$$

where $\cos \alpha$, $\cos \beta$ and $\cos \gamma$ are the direction cosines of the ℓ axis, and ℓ is the distance along the source measured from the endpoint (x_1, y_1,z_1). Let the current distribution on the monopole be

$$I(\ell) = \frac{I_1 \sinh\gamma (d - \ell) + I_2 \sinh \gamma\ell}{\sinh \gamma d} \tag{82}$$

where I_1 and I_2 are the endpoint currents. The far-zone field of this source is

$$E_\theta = (\cos\alpha \cos\theta \cos\phi - \cos\beta \cos\theta \sin\phi - \cos\gamma \sin\theta)\, E_\ell \tag{83}$$

$$E_\phi = (-\cos\alpha \sin\phi + \cos\beta \cos\phi)\, E_\ell \tag{84}$$

where

$$E_\ell = \frac{\eta\, e^{-\gamma r}}{4\pi r\,(1-g^2) \sinh \gamma d} \left[(e^{\gamma g d} - g \sinh \gamma d - \cosh \gamma d)\, I_1\, e^{\gamma f_1} + (e^{-\gamma g d} + g \sinh \gamma d - \cosh \gamma d)\, I_2\, e^{\gamma f_2}\right] \tag{85}$$

$$f_1 = x_1 \sin\theta \cos\phi + y_1 \sin\theta \sin\phi + z_1 \cos\theta \tag{86}$$

(87) $$f_2 = x_2 \sin\theta \cos\phi + y_2 \sin\theta \sin\phi + z_2 \cos\theta$$

(88) $$g = \cos\alpha \sin\theta \cos\phi + \cos\beta \sin\theta \sin\phi + \cos\gamma \cos\theta$$

and (r,θ,ϕ) are the spherical coordinates of the observation point. Although γ denotes the propagation constant and $\cos\gamma$ is a direction cosine, no confusion should arise.

For a sinusoidal V dipole, each monopole has different direction cosines but scalar addition applies to the field components E_θ and E_ϕ of each monopole.